Supplement of Earth Syst. Dynam., 9, 383–391, 2018
https://doi.org/10.5194/esd-9-383-2018-supplement

Earth System Dynamics
Open Access

Supplement of

Quantifying changes in spatial patterns of surface air temperature dynamics over several decades

Dario A. Zappalà et al.

Correspondence to: Cristina Masoller (cristina.masoller@upc.edu)

Abstract. Here we provide supporting information for the results presented in the main text.

In the first section we present an overview of how the Hilbert transform works. This overview is aimed at introducing the method to the readers that are not acquainted with it, and also, it is aimed at explaining our motivation for using this method, and some details of the implementation.

In the second section we apply Hilbert analysis to synthetic data generated with an autoregressive process, and compare the results with those obtained from SAT reanalysis data.

In the third section we discuss how the threshold used for the significance test affects the maps of relative changes, and also, we apply a percentile-based significance test to confirm the validity of our results.

In the fourth section we discuss how the maps obtained depend on the time intervals used to calculate the relative variations. While in the main text we have used the first and final decades of the reanalysis (1979–1988 and 2007–2016), here we compare with the first and final five years (1979–1983 and 2012–2016) and also, with the first half period and the second half period (1979–1997 and 1998– 2016). Maps with very similar spatial structures are found, confirming the robustness of our findings.

Finally, in the last section, we compare the results obtained from two reanalysis datasets (ERA-Interim and NCEP-DOE) and show that Hilbert amplitude and frequency uncover qualitatively similar spatial structures, but there are also some relevant differences between the two reanalysis.

1 Overview of Hilbert transform

The Hilbert transform (HT) provides, for a real signal $x(t)$, an *analytic signal*, $\zeta(t)$, from where an instantaneous amplitude and an instantaneous phase can be defined:

$$\zeta(t) = x(t) + iy(t) = a(t)e^{i\varphi(t)} \tag{1}$$

where $y(t)$ is the Hilbert transform of $x(t)$:

$$y(t) = H[x(t)] = \pi^{-1}\text{P.V.}\int_{-\infty}^{+\infty} \frac{x(\tau)}{t-\tau} d\tau, \tag{2}$$

where P.V. means principal value, and a and φ can be calculated as: $a(t)=\sqrt{[x(t)]^2+[y(t)]^2}$, and $\varphi(t)=\arctan[y(t)/x(t)]$. The series obtained by HT allow us to reconstruct the original series as $x(t)=a(t)\cos\varphi(t)$.

Although formally $a(t)$ and $\varphi(t)$ can be computed for any arbitrary $x(t)$, they have a clear physical meaning only if $x(t)$ is a narrow-band oscillatory signal: in that case, the amplitude $a(t)$ coincides with the envelope of $x(t)$ and the instantaneous frequency, $\omega(t)=d\varphi(t)/dt$, coincides with the frequency of the maximum of the power spectrum computed in a running window (*Pikovsky et al.*, 2001).

As a first example, the Hilbert transform of the harmonic oscillation $x(t)=a\cos(\omega t)$ is $y(t)=a\sin(\omega t)$. In the complex plane, $(x(t),y(t))$ represent the coordinates of a point that describes a circular trajectory of amplitude a and phase ωt.

As a second example, we calculate the instantaneous amplitude and frequency of the oscillation described by

$$x(t)=\mathrm{e}^{-\alpha t}\cos\left[\omega_0\left(1+\mathrm{e}^{-2\alpha t}\right)t\right]. \tag{3}$$

We choose $\omega_0=2\pi/400$, $\alpha=2/T$ with $T=10^5$ being the length of the time series. To calculate the HT we use (as in the main text) the algorithm proposed in Bilato et al. (2014). The results are shown in Figure 1. We can see that the amplitude $a(t)$ is the exponentially decreasing envelope of $x(t)$, while the frequency $\omega(t)$ has a temporal evolution which is consistent with the expression of $x(t)$. We also note that near the extremes $a(t)$ and $\omega(t)$ display a small oscillatory behaviour.

To better understand the magnitude of this effect, we take into account a simple harmonic oscillation $x(t)=\cos(\omega_0 t)$ with $\omega_0=2\pi/400$. In Figure 2 we show the results of Hilbert analysis over this time series $x(t)$. We see that the amplitude $a(t)$ is the envelope of the series $x(t)$, however, a closer inspection (in panel b) reveals small oscillations near the beginning and near the end of the time series. In the same way, the instantaneous frequency $\omega(t)$ is not always exactly equal to the theoretical frequency ω_0, but displays oscillations near the extremes. In other words, near the extremes of the series, even if the reconstruction $x(t)=a(t)\cos\varphi(t)$ still exactly holds (within the numerical precision), the values of amplitude, phase and frequency, taken separately, deviate from the true values. So, for our work we chose to disregard the initial and the final 5% of the time series, as we have tested (with various examples, by comparing the numerical HT with the known analytical HT) that this choice gives a relative error of amplitude and frequency which is lower than 1%.

2 Hilbert analysis of synthetic data

In order to gain insight into the results obtained from SAT time series, we generated synthetic time series aimed at mimicking real SAT data, but with a parameter, α, that allows to control the level of noise.

As a minimal model of SAT time series we consider the sum of a sinusoidal term and a stochastic term that is an autoregressive (AR) process of order one. We have chosen an AR model because it is commonly used in the literature to model climate data (*Hasselmann*, 1976).

$$S(t)=\sqrt{1-\alpha}\sqrt{2}\sin(\omega_0 t)+\sqrt{\alpha}\xi(t). \tag{4}$$

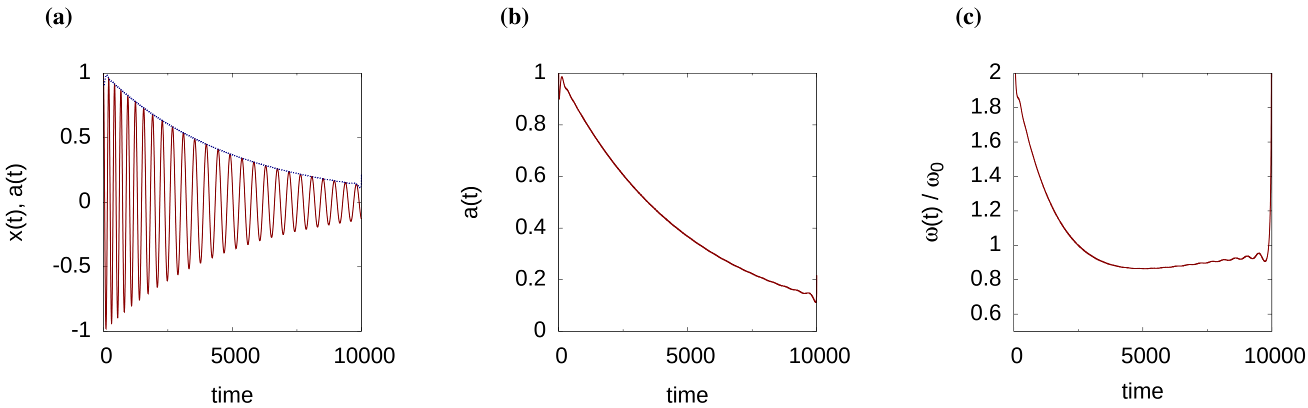

Figure S1. Hilbert analysis applied to the time series with time-varying amplitude and frequency given by Eq.(3). (**a**) Time series $x(t)$ (red line) and its Hilbert amplitude $a(t)$ (blue line); (**b**) Hilbert amplitude $a(t)$; (**c**) ratio between the instantaneous Hilbert frequency and ω_0.

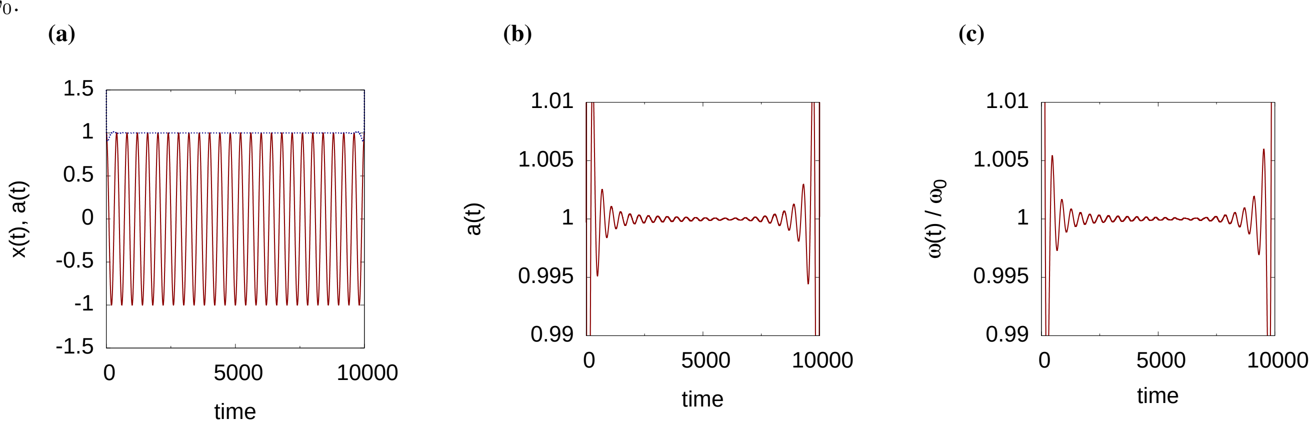

Figure S2. As Fig. 1, but for the harmonic time series $x(t) = \cos(\omega_0 t)$.

By choosing $\omega_0 = 2\pi/365$ oscillations/day, the sinusoidal term can mimic an annual oscillation with daily resolution. Here $\sqrt{2}$ is a normalisation factor chosen so that $\sqrt{2}\sin(\omega_0 t)$ has unit variance. $\xi(t)$ is an AR(1) process with zero mean and unit variance (the parameter that expresses the persistence of the noise is $\beta = 0.5$). The control parameter $\alpha \in [0,1]$ allows to vary the level of noise, while keeping constant the first and second moments of the distribution of $S(t)$ values (zero mean and unit variance). Synthetic time series are generated according to Eq. (4), with the same length as ERA daily reanalysis: $T = 13696$ days. From the synthetic time series we calculate the instantaneous Hilbert amplitude and frequency, following the same procedure as for the real SAT time series.

Figures 3(a) and 3(b) display the results obtained from synthetic series, the average amplitude and frequency respectively, as a function of α, with error bars that represent standard deviations. These results were computed from 10 realizations of the

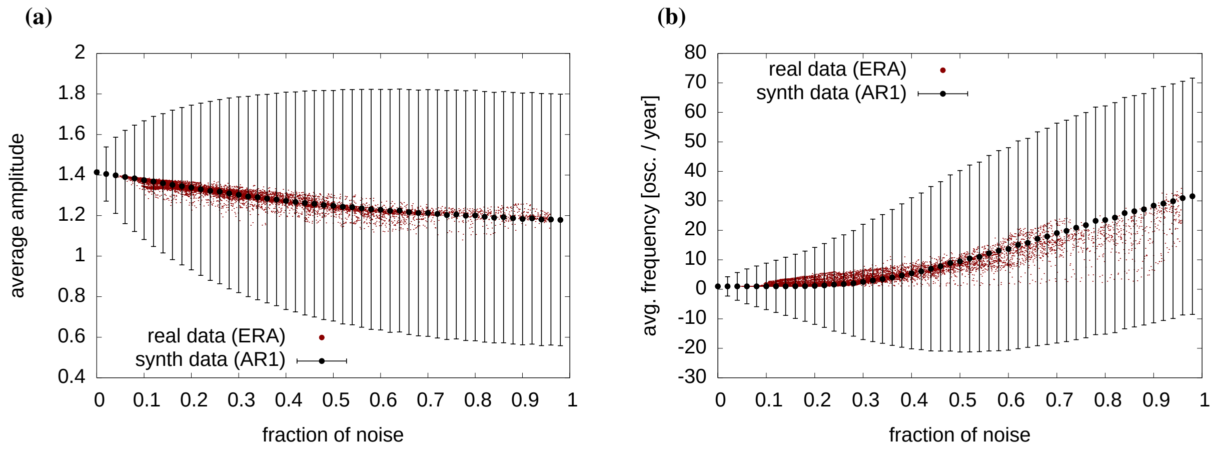

Figure S3. Comparison between real SAT series and synthetic series. (**a**) Average amplitude and (**b**) average frequency as a function of level of noise, α, in Eq. (4). The error bars are computed from 10 realizations of the AR(1) process. The red dots indicate the values computed from real SAT data.

AR(1) process for each value of α. For comparison, the values obtained from SAT time series are also displayed (red dots). We can see that there is a very good agreement between synthetic and SAT results, which suggests that, as a minimal model, we can consider SAT time series as the sum of a regular oscillation and an irregular noisy term represented by an AR process. As we have shown in *Zappalà et al.* (2016), the regular term tends to prevail in the extratropics, while the noisy term prevails in the tropics and in some specific extratropical areas. In the synthetic data we note that, as the noise level increases, the average Hilbert frequency increases while the average Hilbert amplitude decreases, a trend that is also observed in real SAT time series: the larger the average amplitude, the lower the average frequency. This trend can be understood by considering the limiting values of α: if $\alpha = 0$, Eq. (4) is just a sine normalised to have unit variance, which gives an amplitude ≈ 1.4; if $\alpha = 1$, Eq. (4) is fully random, with a Gaussian distribution of unit variance that gives an amplitude ≈ 1.1.

3 Significance test

As we explained in the main text, we performed a significance test on the maps of relative change of the calculated quantities. We calculated 100 surrogate values of the same relative change, and from this ensemble we calculated the average μ and the standard deviation σ. Then, we considered the actual (no surrogate) relative change as statistically significant if its distance from μ is at least 2σ.

To see in more details how this technique works, in Figure 4 we show examples of the maps of change of amplitude and frequency, with different choices of the threshold value. As expected, we see that the higher the threshold is, the more sites get erased from the map. Nonetheless, the main structures are still present even at 4σ, so we can conclude that they are robust with respect to the significance filtering.

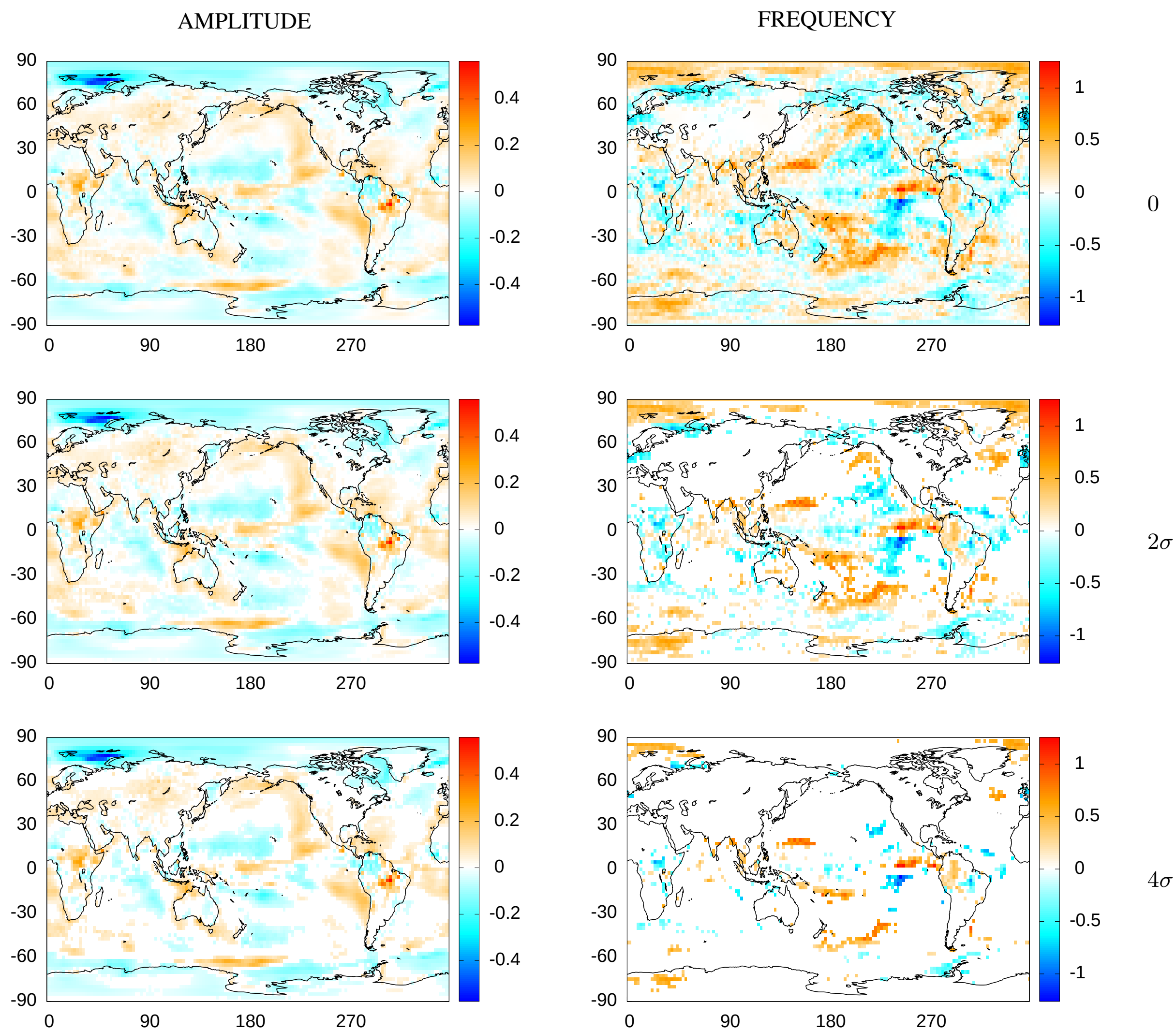

Figure S4. Maps of relative change of amplitude (left column) and frequency (right column), with different values for the significance filter. First row: no filter. Second row: only values with a distance of at least 2σ from the average of the 100 surrogate values. Third row: as the second one, but with a threshold of 4σ.

An alternative significance test is based on the *percentile* of the values obtained from surrogated series. For example, we can consider a result (i.e., a relative change value) as statistically significant if it lies out of the range of the 95% central surrogate results. In Figure 5 we present the maps of relative change of average amplitude (left) and of average frequency (right) obtained by using this criterion. A comparison with the two maps in Fig. 4 for threshold 2σ confirms that very similar spatial patterns are uncovered.

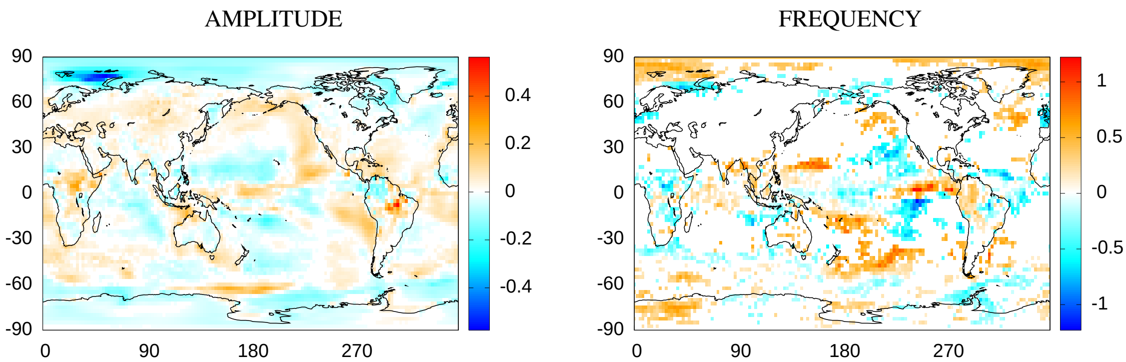

Figure S5. Maps of relative change of average amplitude (left) and of average frequency (right) obtained with the 95% percentile-based significance filter, computed with 100 surrogates.

4 Influence of the time intervals used to calculate the relative variations

Here we analyze how the regions where significant changes are uncovered depend on the time period considered to calculate the relative variations. While in the main text we have used the first and final decades of the reanalysis (1979–1988 and 2007–2016), here we compare with the first and final five years (1979–1983 and 2012–2016) and also, with the first half period and the second half period (1979–1997 and 1998–2016).

The results are shown in Fig. 6, where the left column displays the changes of average amplitude, the right column of average frequency, the first row displays changes between the first and last 5 years, the second row between the first and last 10 years (as in the main text), and in the third row, between the first half and the second half of the total period. We can see that, in the amplitude maps, the structures are robust and in particular, the blue spot in the Arctic and the red spot in the Amazonia are present in the three maps. In the frequency maps, the dipole in the east Pacific Ocean and the red areas in the west Pacific Ocean are also present in the three maps. While the spatial structures are very robust with respect to the time interval considered, the magnitude of the relative changes depends on the time interval, and the variations are (as could be expected) smaller when they are computed between the first half and the second half of the total period (third row).

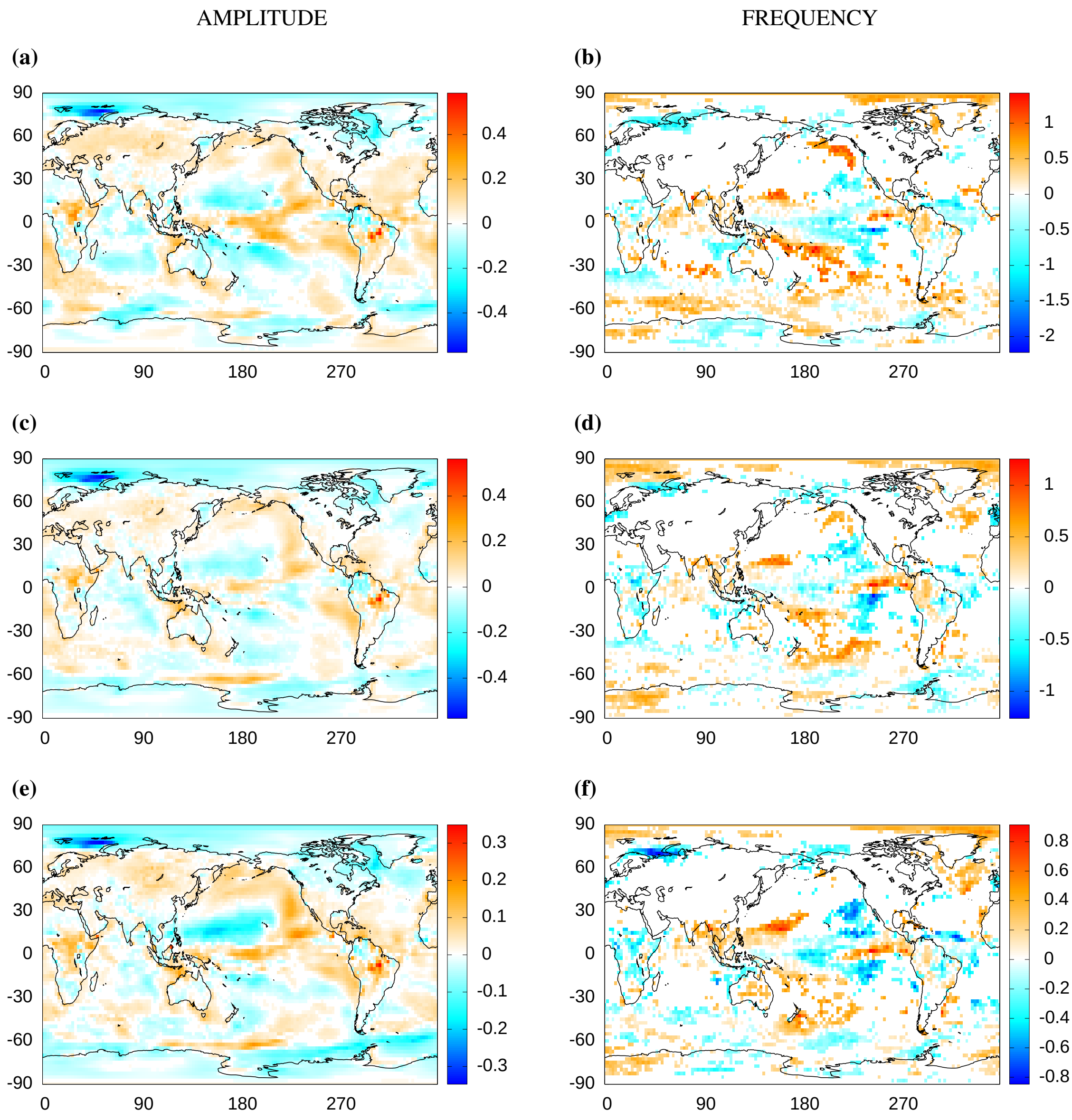

Figure S6. Variation of average amplitude (left) and of average frequency (right), calculating the relative change between (**a**, **b**): the first and the last 5 years; (**c**, **d**): the first and the last 10 years (as in the main text); (**e**, **f**): the first half and the second half of the time series.

5 Comparison between ERA-Interim and NCEP-DOE reanalysis

To test the robustness of our findings, in Fig. 7 we compare the maps of relative change of amplitude and frequency, obtained from two daily reanalysis datasets: ERA-Interim and NCEP-DOE Reanalysis 2. NCEP-DOE covers a longer period and has $94 \times 192 = 18048$ geographical sites. In order to perform a precise comparison between the results of the two datasets, in the NCEP-DOE Reanalysis we consider the same time period as the ERA-Interim dataset.

In the first row (a,b) we present the maps of change of average amplitude, while in the second row (c,d) we have the maps of change of amplitude variance. A qualitative good agreement of spatial structures is seen, however, some differences can be noticed, such as in the Indian Ocean, where NCEP-DOE reanalysis (panel b) gives an increase of average amplitude, while ERA (panel a) gives a decrease.

The third and fourth rows present the maps of change of average frequency and of frequency variance. Here we can again see a qualitative agreement, but there are also some relevant differences. To investigate the underlying reasons, we inspected the time series in selected regions in which the differences between maps (e) and (f) are more pronounced (for example, one map shows a small change while the other one shows a large change). We found that there were indeed significant differences between the two SAT time series, in the same geographical region. As an example, Fig. 8 displays the two SAT series in the region that is marked in South America. We see that the time series from ERA-Interim dataset maintains the same general trend throughout the entire length. On the other hand, the NCEP-DOE time series has a sudden change around year 2000, when the seasonal cycle becomes significantly smaller and the rapid fluctuations get a more dominant role on the series. Therefore, Hilbert frequency is sensitive to this change and detects this difference between the two datasets, which should be due to different models used to perform the reanalysis.

Therefore, Hilbert analysis is a useful data analysis tool for performing model inter-comparisons, because it captures temporal variations of amplitude and frequency that may not be detected by other analysis tools. It is an open question which reanalysis more closely represents the real SAT values.

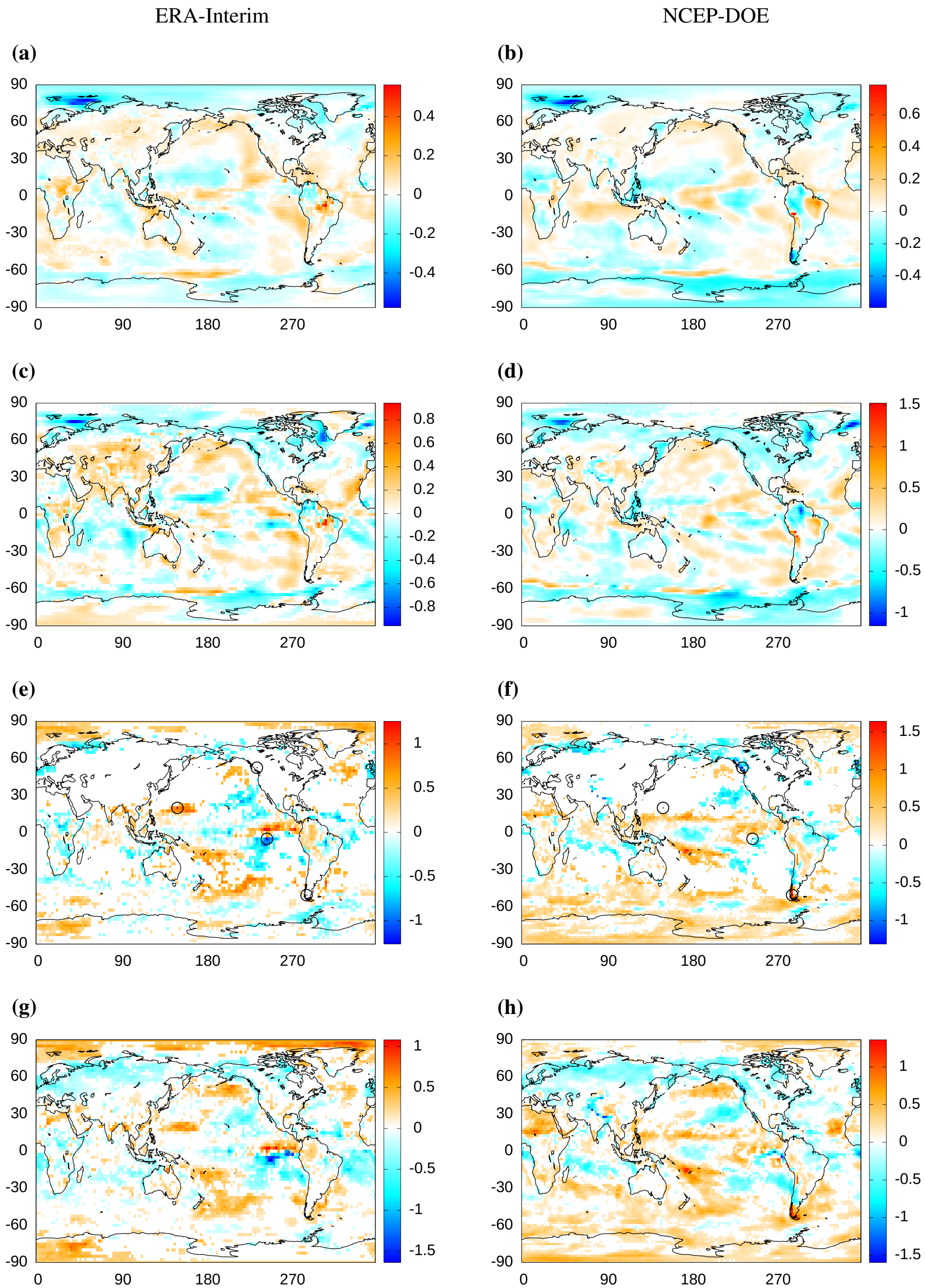

Figure S7. Comparison of results obtained from ERA-Interim (left) and NCEP-DOE (right). Relative change of (**a**, **b**) average amplitude; (**c**, **d**) amplitude variance; (**e**, **f**) average frequency; (**g**, **h**) frequency variance.

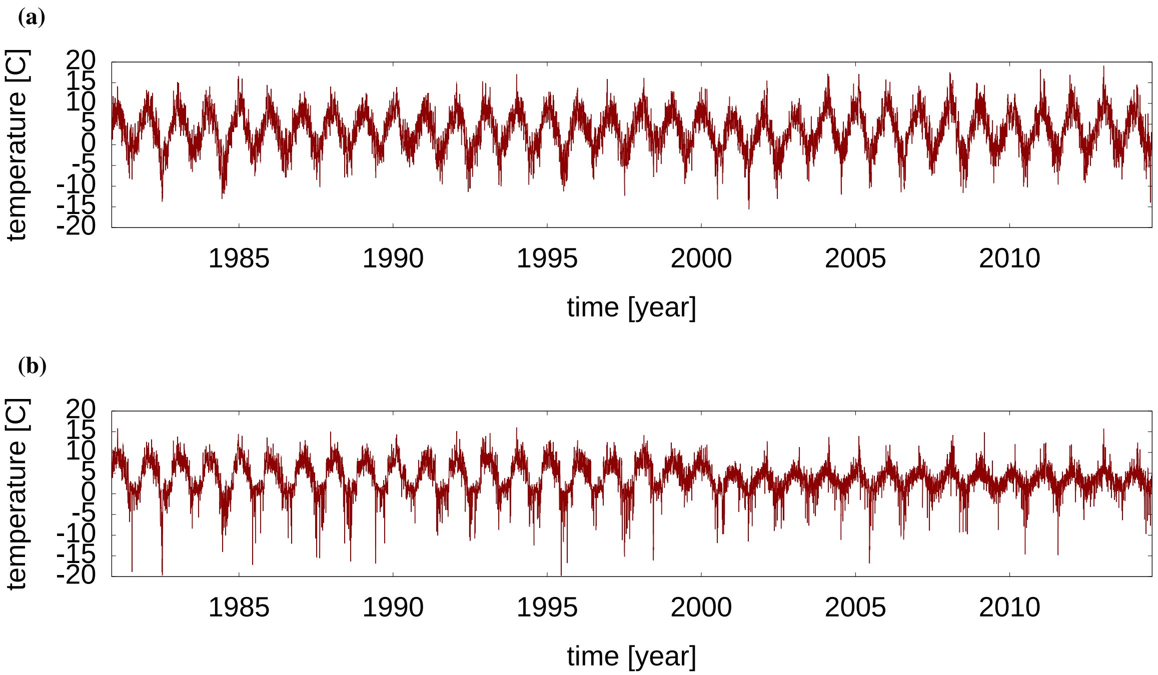

Figure S8. Comparison between SAT series of the same point (50 S, 287.5 E) in the two datasets: (**a**) in ERA-Interim and (**b**) in NCEP-DOE.

References

Pikovsky, K.; Rosenblum, M.; Kurths, J. *Synchronization: A universal concept in nonlinear sciences.* Cambridge University Press (2001).

Bilato, R., O. Maj, and M. Brambilla: An algorithm for fast Hilbert transform of real functions, Adv. Comput. Math., 40, 1159–1168, 2014.

Hasselmann, K. *Stochastic climate models part I: Theory.* Tellus (1976) 28, 473.

Zappalà, D. A. et al. *Global atmospheric dynamics investigated by using Hilbert frequency analysis.* Entropy (2016) 18 (11): 408.